

# Efficient Ultra-Broadband C-to-O Band Converter Based on Multi-Mode Silicon-on-Insulator Waveguides

G. Ronniger<sup>(1, 4)</sup>, I. Sackey<sup>(1, 2)</sup>, T. Kernetzky<sup>(3)</sup>, U. Höfler<sup>(3)</sup>, C. Mai<sup>(4)</sup>, C. Schubert<sup>(2)</sup>,  
N. Hanik<sup>(3)</sup>, L. Zimmermann<sup>(1, 4)</sup>, R. Freund<sup>(1, 2)</sup>, K. Petermann<sup>(1)</sup>

<sup>(1)</sup> Technische Universität Berlin (TUB), Einsteinufer 25, 10587 Berlin, Germany

<sup>(2)</sup> Fraunhofer Institute for Telecommunications (HHI), Einsteinufer 37, 10587 Berlin, Germany

<sup>(3)</sup> Technical University of Munich (TUM), Arcisstraße 21, 80333 München, Germany

<sup>(4)</sup> IHP GmbH, Im Technologiepark 25, 15236 Frankfurt (Oder), Germany

[g.ronniger@tu-berlin.de](mailto:g.ronniger@tu-berlin.de), [isaac.sackey@hhi.fraunhofer.de](mailto:isaac.sackey@hhi.fraunhofer.de), [tasnad@tum.de](mailto:tasnad@tum.de)

**Abstract** We present a novel all-optical wavelength converter based on inter-modal FWM in a *p-i-n*-diode-assisted SOI integrated waveguide that is capable of converting wavelengths from the entire C band to the O band. 32 Gbd QPSK converted signals were experimentally transmitted over 100 km.

## Introduction

Currently, we see an increasing interest in fully utilizing the optical bandwidth of a standard single-mode fiber (SSMF) in multi-band transmission systems<sup>[1]–[3]</sup> to keep up with the envisaged capacity demand. Also, coherent transmission in the O band becomes more practical in data centers<sup>[4]</sup> with the corresponding growth in traffic.

The use of all-optical wavelength converters (AOWCs) is beneficial in both of these scenarios. In the first one, it acts as a bridge between long-haul C-band networks and shorter-range O-band networks. Approaches based on electronics typically suffer from disadvantageous scaling of power and complexity with respect to channel count, symbol rate and modulation format, while the all-optical solution is fully transparent to all of those parameters. In another application, different parallel AOWCs (each one optimized for a particular band) can be used with available efficient C-band equipment (not fully available outside of the C band) to process multi-band signals filling the entire spectrum from O to L bands.

In general, AOWCs have been realized in highly nonlinear fibers<sup>[5]</sup>, silicon<sup>[6]</sup>, silicon nitride<sup>[7]</sup> and other integrated platforms<sup>[8]</sup>, and more recently, using inter-modal four-wave mixing (FWM) in few-mode fibers<sup>[9]</sup> and silicon-based multi-mode waveguides (MMWGs)<sup>[10],[11]</sup> to enable larger wavelength translations. Numerical simulations on novel nonlinear materials even predict conversion bandwidths up to 750 nm in single-mode waveguides<sup>[12]</sup>. However, experimental all-optical conversion of data signals between C and O

band has only attracted little attention so far. The previous implementations either only demonstrated a single channel<sup>[13]</sup> or required a change in pump wavelength to convert multiple channels<sup>[14]</sup>. Therefore, to the best of our knowledge, this is the first system demonstration of an integrated device, capable of all-optically converting the complete C band into the O band at once.

## Wavelength Converter Design

To implement the actual wavelength converter, we employ a photonic integrated circuit (PIC) design, as shown in Fig. 1, fabricated using IHP's Photonic BiCMOS technology<sup>[15]</sup>. The MMWG is connected to an on-chip mode-multiplexing and -demultiplexing unit at the input and output, respectively. Those contain an O-band grating coupler (GC) optimized for 1310 nm, connected to a tapered waveguide yielding the fundamental mode ( $TE_0$ ) of the MMWG. Further, a C-band GC, optimized for 1550 nm, is connected to a mode add-drop multiplexer (MADM), designed to couple the  $TE_0$  signal from the GC into the  $TE_1$  mode of the MMWG. For those components, we rely on previous designs: the GCs are standard building blocks of the technology, the MADMs are from a previous PIC<sup>[10]</sup>, with minor modifications. The MMWG itself was designed as a rib waveguide to allow for a *p-i-n* diode, which is used to remove free carriers created by two-photon absorption and subsequent free-carrier absorption. The

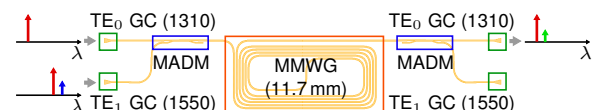


**Fig. 1:** Structure of proposed PIC and simplified spectra of FWM process with pump (red), signal (blue) and idler (green).

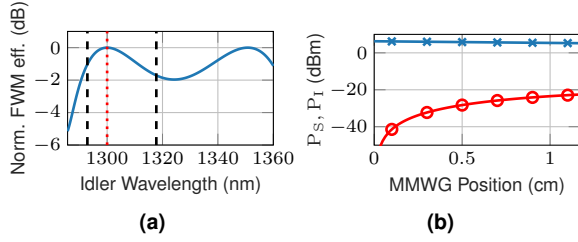


**Fig. 2:** Normalized FWM efficiency for the designed waveguide (a). Region from Fig. 4a (black dashed) and the O-band pump (red dotted) are indicated. Simulated power evolution of signal (blue crosses) and idler (red circles) along the waveguide for signal at 1548 nm (b). Initial pump and signal powers include 5 dB input MADM / GC losses.

MMWG's length is designed to be 11.7 mm and bends were designed to be adiabatic<sup>[16]</sup>.

Although the batch of chips used here is from a generation manufactured before extensive phase matching optimizations<sup>[17]</sup> were performed, we found that for standard slab height 100 nm, the chips with rib width 1672 nm are very close to the optimum. Fig. 2a shows the normalized FWM efficiency  $|\eta|/\max(|\eta|)$  for this particular design, which measures how much the idler amplitude is reduced due to phase mismatch. FWM efficiency is defined as<sup>[18]</sup>  $\eta = (1 - \exp(-(\alpha + j\Delta\beta)L)) / ((\alpha + j\Delta\beta)L)$  with phase mismatch  $\Delta\beta$ , waveguide length  $L$  and attenuation  $\alpha$ . Fig. 2b shows the on-chip idler power evolution for operating conditions like in the following system experiment, simulated by solving propagation differential equations with an Adams-Bashforth-Moulton solver. Therefore, we expect an input-output conversion efficiency (CE) – defined as ratio of idler power at fiber output to signal power at fiber input – of about  $-39$  dB (incl. 5 dB MADM / GC losses at both in- and output).

### Experimental Setup

Figure 3 shows the setup used for the following measurements. It consists of the transmitter, the AOWC stage, the transmission stage and finally a Kramers-Kronig receiver (KK-Rx). The transmitter was used to generate a 32 Gbd single-polarization quadrature phase-shift keying (QPSK) signal. In the AOWC, this signal was combined with pump 2. This combination was sent to the  $TE_1$  input of the PIC, while pump 1 was connected to  $TE_0$ . The pumps are amplified by an Erbium-doped fiber amplifier (EDFA) / Praseodymium-doped fiber amplifier (PDFA), power-controlled by a variable optical attenuator (VOA) and filtered by a tunable optical band-pass filter (T-OBPF). The PIC was temperature controlled and reverse biased with 20 V. The output coupling angle was optimized for flat CE. Then,

pump and signal polarizations and the fiber-to-chip coupling were optimized for high CE. From the  $TE_0$  output, the idler is either sent through a noise-loading stage or over a 100 km SSMF link.

Due to unavailability of a coherent O-band receiver, a KK-Rx was used. It adds a polarization-aligned offset continuous wave (CW) carrier to the signal and uses their beating on a photo diode (PD) to retrieve the complex base band in the digital domain. Afterwards, it can be processed by conventional digital signal processing (DSP)<sup>[19]</sup>. By adjusting the CW carrier PDFA, the carrier-to-signal power ratio was maintained at 13.5 dB. The CW carrier wavelength was placed to create a guard band of 1.8 GHz between the carrier and the received signal. The T-OBPF in the KK-Rx was adjusted to minimize the bit error rate (BER).

### Experimental Results

For the following experiments, the powers, measured at the PIC's input, were 11.3 dBm, 24.0 dBm and 19.3 dBm for signal, pump 1 and pump 2, respectively. Starting at optimal simulated values, we iteratively refined the pump wavelengths for large bandwidth and high CE. Finally, pump wavelengths of 1540 nm and 1300 nm for pump 1 and 2, respectively, were used for efficient broadband operation (i.e. we employ a wavelength translation by 240 nm – a value seldomly achieved in previous experimental works).

In a first CW FWM characterization, the transmitter was replaced by a tunable external-cavity laser (ECL). Figure 4a shows the measured CE when this ECL's wavelength is swept from 1530 nm to 1565 nm and all other conditions stay the same. From this figure, we measure a peak CE of  $-41$  dB (close to the simulated value of  $-39$  dB) and a bandwidth of at least 25 nm in the C band, while there is no indication of declining efficiency toward higher wavelengths. When a pump inside the band is acceptable, even the complete C band's bandwidth of 35 nm can be converted. Although our measurement was unfortunately restricted to the C band due to unavailable equipment, our phase matching simulation suggests a much higher bandwidth of up to almost 100 nm (see Fig. 2a). However, in the current device this would be limited by the GC 1 dB-bandwidth of approximately 30 nm. We assume that the ripple in the measured CE is due to inter-modal crosstalk. Based on these results, we performed C-to-O conversion experiments using data signals with wavelengths of 1542 nm, 1548 nm and 1562 nm,

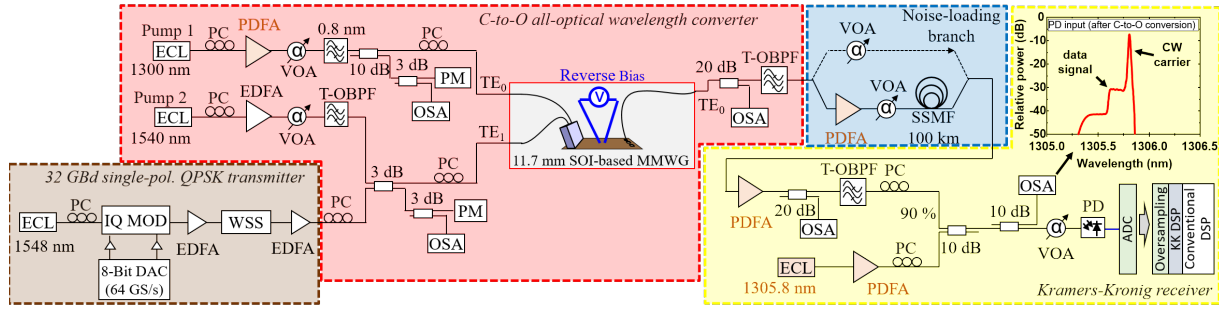


**Fig. 3:** Experimental setup for C-to-O conversion, including transmitter stage (brown box), AOWC stage (red box), noise-loading or optional transmission stage (blue box) and KK-Rx stage, including optical spectrum at photo diode as inset (yellow box).

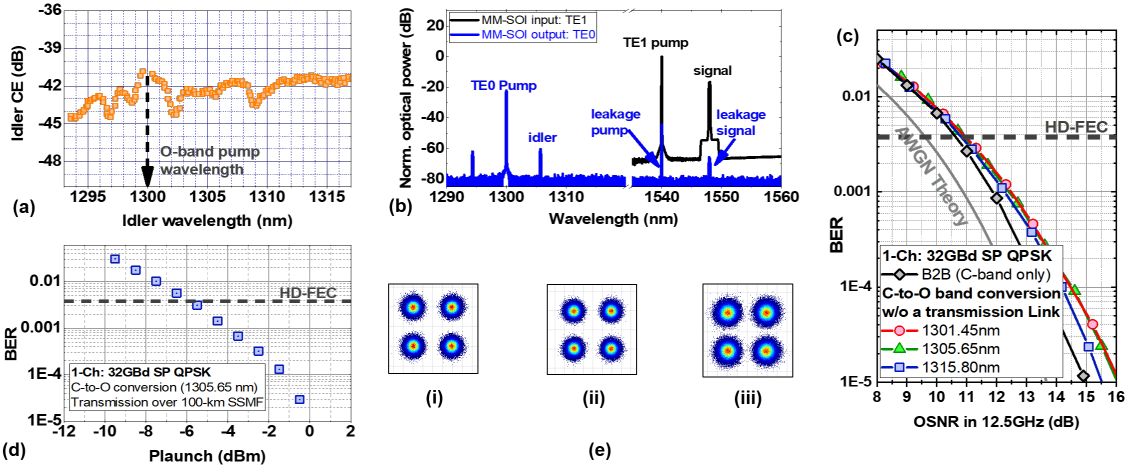


**Fig. 4:** Experimental results of the AOWC pumped by 24.0 dBm at 1540 nm and 19.3 dBm at 1300 nm: Measured CW CE for signals in C band (a). Spectra at the PIC input and output (b). BER of 32 Gbd single-polarization (SP) QPSK signals, received after noise-loading stage (c) and after 100 km SSMF using different launch powers for signal at 1548 nm (d). Constellation diagrams (e) after the transmitter (i), after the AOWC (ii) and after transmission over 100 km SSMF (iii).

with an additional back to back (B2B) experiment at 1548 nm. In the B2B case, the transmitter was directly connected to the noise loading stage and T-OBPF, ECL and PDFA in the KK-Rx were replaced by their respective C-band counterparts. The results are summarized in Fig. 4c, which indicates an optical signal to noise ratio (OSNR) penalty of less than 0.4 dB at the hard-decision forward error correction (HDFEC) threshold from the AOWC with respect to the B2B case. For this figure, the OSNR was corrected to a noise bandwidth of 12.5 GHz, to make C-band and O-band measurements comparable. Finally, for the 1548 nm channel, the noise-loading stage was replaced by a 100 km SSMF transmission link (35 dB insertion loss). A VOA was used to change the launched powers of the converted signals. For each power, the BER was measured and the result is shown in Fig. 4d. A launch power of only  $-5.5$  dBm is sufficient to stay below the HDFEC threshold after 100 km.

According to Fig. 4b, pump 1 still has significant power at the output of the AOWC. Even though a T-OBPF suppressed this pump by about 30 dB, it still dominated the output of the following PDFA. Therefore, only limited launch power for the con-

verted signal was feasible in the transmission experiment. For later devices, we plan to integrate on-chip pump filtering to clean the output.

Additionally, Fig. 4e shows the measured constellations after the transmitter, after the AOWC and after transmission over 100 km, each at highest OSNR achieved. No relevant distortion is visible after the AOWC. Therefore, we assume that other modulation formats work as well.

## Conclusions

An integrated AOWC, capable of converting the complete C band into the O band, has been realized for the first time. It employed inter-modal FWM in a p-i-n-diode-assisted MMWG to achieve a CE of  $-41$  dB at moderate pump powers. For all tested channels, the AOWC caused an OSNR penalty below 0.4 dB, and the performance was verified by transmission over 100 km SSMF for a single channel. Using a PIC platform enabled on-chip integration of MADMs and allows for space- and cost-efficient extensions, infeasible in fiber-based approaches.

## Acknowledgments

This work was supported by the DFG projects PE 319/36-2, ZI 1283/3-2, HA 6010/6-1, ZI 1283/5-1 and FR 851/3-1.

## References

- [1] D. Uzunidis, E. Kosmatos, C. Matrakidis, A. Stavdas, and A. Lord, "Strategies for upgrading an operator's backbone network beyond the C-band: Towards multi-band optical networks", *IEEE Photonics Journal*, vol. 13, no. 2, pp. 1–18, Apr. 2021, ISSN: 1943-0655, 1943-0647. DOI: 10.1109/JPHOT.2021.3054849.
- [2] A. Ferrari, A. Napoli, J. K. Fischer, N. Costa, A. D'Amico, J. Pedro, W. Forysiak, E. Pincemin, A. Lord, A. Stavdas, J. P. F.-P. Gimenez, G. Roelkens, N. Calabretta, S. Abrate, B. Sommerkorn-Krombholz, and V. Curri, "Assessment on the achievable throughput of multi-band ITU-T G.652.D fiber transmission systems", *Journal of Lightwave Technology*, vol. 38, no. 16, pp. 4279–4291, Aug. 15, 2020, ISSN: 0733-8724, 1558-2213. DOI: 10.1109/JLT.2020.2989620.
- [3] N. Sambo, A. Ferrari, A. Napoli, N. Costa, J. Pedro, B. Sommerkorn-Krombholz, P. Castoldi, and V. Curri, "Provisioning in multi-band optical networks", *Journal of Lightwave Technology*, vol. 38, no. 9, pp. 2598–2605, May 1, 2020, ISSN: 0733-8724, 1558-2213. DOI: 10.1109/JLT.2020.2983227.
- [4] P. M. Seiler, A. Peczek, G. Winzer, K. Voigt, S. Lischke, A. Fatemi, and L. Zimmermann, "56 GBaud O-band transmission using a photonic BiCMOS coherent receiver", in *2020 European Conference on Optical Communications (ECOC)*, Brussels, Belgium: IEEE, Dec. 2020, Tu2C-4, ISBN: 978-1-72817-361-0. DOI: 10.1109/ECOC48923.2020.9333218.
- [5] S. Singh, S. Singh, Q. M. Ngo, and A. M. Mohammadi, "Analysis of all-optical wavelength converter based on FWM effect in HNLF for coherent 100 Gbps dual-polarized DQPSK signal", *Optical Fiber Technology*, vol. 59, p. 102323, Oct. 1, 2020, ISSN: 1068-5200. DOI: 10.1016/j.yofte.2020.102323.
- [6] P. Girouard, L. H. Frandsen, M. Galili, and L. K. Oxenløwe, "Record-high continuous-wave nonlinear performance of amorphous silicon waveguides", in *Conference on Lasers and Electro-Optics*, Washington, DC: OSA, 2020, SW3N.5, ISBN: 978-1-943580-76-7. DOI: 10.1364/CLEO\_SI.2020.SW3N.5.
- [7] G. F. R. Chen, J. W. Choi, Y. M. Cao, D. K. T. Ng, and D. T. H. Tan, "Parametric wavelength conversion of 30Gbps NRZ data in ultra-silicon-rich nitride waveguides", in *14th Pacific Rim Conference on Lasers and Electro-Optics (CLEO PR 2020)*, Sydney: OSA, 2020, C5C\_4, ISBN: 978-0-646-82504-5. DOI: 10.1364/CLEOPR.2020.C5C\_4.
- [8] D. Kong, M. Pu, Y. Liu, Y. Zheng, E. Semenova, K. Yvind, L. K. Oxenløwe, M. Galili, and H. Hu, "Wavelength conversion of 10 Gbit/s data from 2000 to 1255 nm using an AlGaAsOI nanowaveguide and a continuous-wave pump in the C band", in *Optical Fiber Communication Conference (OFC) 2019*, San Diego, California: OSA, 2019, W4F.3, ISBN: 978-1-943580-53-8. DOI: 10.1364/OFC.2019.W4F.3.
- [9] G. Rademacher, R. S. Luis, B. J. Puttnam, Y. Awaji, M. Suzuki, T. Hasegawa, H. Furukawa, and N. Wada, "Wideband intermodal nonlinear signal processing with a highly nonlinear few-mode fiber", *IEEE Journal of Selected Topics in Quantum Electronics*, vol. 26, no. 4, pp. 1–7, Jul. 2020, ISSN: 1077-260X, 1558-4542. DOI: 10.1109/JSTQE.2020.2984563.
- [10] G. Ronniger, S. Lischke, C. Mai, L. Zimmermann, and K. Petermann, "Investigation of inter-modal four wave mixing in p-i-n diode assisted SOI waveguides", in *2020 IEEE Photonics Society Summer Topicals Meeting Series (SUM)*, Cabo San Lucas, Mexico: IEEE, 2020, TuD2.3, ISBN: 978-1-72815-887-7. DOI: 10.1109/SUM48678.2020.9161068.
- [11] S. Signorini, M. Finazzer, M. Bernard, M. Ghulinyan, G. Pucker, and L. Pavesi, "Silicon photonics chip for inter-modal four wave mixing on a broad wavelength range", *Front. in Phys.*, vol. 7, p. 128, Sep. 13, 2019, ISSN: 2296-424X. DOI: 10.3389/fphy.2019.00128.
- [12] Y. Liu, M. Galili, K. Yvind, L. K. Oxenløwe, H. Hu, and M. Pu, "High-order phase-matching enabled octave-bandwidth four-wave mixing in AlGaAs-on-insulator waveguides", in *Conference on Lasers and Electro-Optics*, San Jose, California: OSA, 2019, JTu2A.83, ISBN: 978-1-943580-57-6. DOI: 10.1364/CLEO\_AT.2019.JTu2A.83.
- [13] J. Turkiewicz, G. Khoe, and H. de Waardt, "All-optical 1310 to 1550 nm wavelength conversion by utilising nonlinear polarisation rotation in semiconductor optical amplifier", *Electronics Letters*, vol. 41, no. 1, p. 29, 2005, ISSN: 00135194. DOI: 10.1049/e1:20057435.
- [14] J. Chen and S. Gao, "Wavelength-assignable 1310/1550 nm wavelength conversion using completely phase-matched two-pump four-wave mixing in a silicon waveguide", *Opt. Commun.*, vol. 356, pp. 389–394, Dec. 2015, ISSN: 00304018. DOI: 10.1016/j.optcom.2015.08.014.
- [15] L. Zimmermann, "Monolithic electronic-photonic co-integration in photonic BiCMOS", in *ECOC 2016; 42nd European Conference on Optical Communication*, Sep. 2016.
- [16] C. J. Oton, O. Lemonnier, M. Fournier, and C. Kopp, "Adiabatic bends in silicon multimode waveguides", in *2016 IEEE 13th International Conference on Group IV Photonics (GFP)*, Aug. 2016, pp. 108–109. DOI: 10.1109/GROUP4.2016.7739093.
- [17] T. Kernetzky, Y. Jia, and N. Hanik, "Multi dimensional optimization of phase matching in multimode silicon nano-rib waveguides", in *Photonic Networks; 21st ITG-Symposium*, Leipzig, Germany, 2020, ISBN: 978-3-8007-5423-6.
- [18] K. O. Hill, D. C. Johnson, B. S. Kawasaki, and R. I. MacDonald, "CW three-wave mixing in single-mode optical fibers", *J. Appl. Phys.*, vol. 49, pp. 5098–5106, 1978, ISSN: 0021-8979, 1089-7550. DOI: 10.1063/1.324456.
- [19] I. Sackey, R. Elschner, C. Schmidt-Langhorst, R. Emmerich, and C. Schubert, "Practical trade-offs for Kramers-Kronig reception", in *Photonic Networks; 19th ITG-Symposium*, Jun. 2018.